Phys. Lett. B 853 (2024) 138661

Contents lists available at ScienceDirect

Physics Letters B

journal homepage: www.elsevier.com/locate/physletb

Letter

Constraining nucleon effective masses with flow and stopping observables from the SπRIT experiment

C.Y. Tsang [a,b,c,**], M. Kurata-Nishimura [d,***], M.B. Tsang [a,b,*], W.G. Lynch [a,b,*], Y.X. Zhang [e], J. Barney [a,b], J. Estee [a,b], G. Jhang [a], R. Wang [a], M. Kaneko [d,f], J.W. Lee [g], T. Isobe [d,***], T. Murakami [d,f,***], D.S. Ahn [d], L. Atar [h,i], T. Aumann [h,i], H. Baba [d], K. Boretzky [i], J. Brzychczyk [j], G. Cerizza [a], N. Chiga [d], N. Fukuda [d], I. Gasparic [d,k,h], B. Hong [g], A. Horvat [h,i], K. Ieki [l], N. Inabe [d], Y.J. Kim [m], T. Kobayashi [n], Y. Kondo [o], P. Lasko [p], H.S. Lee [m], Y. Leifels [i], J. Łukasik [p], J. Manfredi [a,b], A.B. McIntosh [q], P. Morfouace [a], T. Nakamura [o], N. Nakatsuka [d,f], S. Nishimura [d], H. Otsu [d], P. Pawłowski [p], K. Pelczar [j], D. Rossi [h,i], H. Sakurai [d], C. Santamaria [a], H. Sato [d], H. Scheit [h], R. Shane [a], Y. Shimizu [d], H. Simon [i], A. Snoch [r], A. Sochocka [j], T. Sumikama [d], H. Suzuki [d], D. Suzuki [d], H. Takeda [d], S. Tangwancharoen [a,s,t], H. Törnqvist [h,i], Y. Togano [l], Z.G. Xiao [u], S.J. Yennello [q,v], Y. Zhang [u], SπRIT collaboration

[a] Facility for Rare Isotope Beams, Michigan State University, East Lansing, MI 48824, USA
[b] Department of Physics, Michigan State University, East Lansing, MI 48824, USA
[c] Kent State University, 800 E Summit St, Kent, OH, 44240, USA
[d] RIKEN Nishina Center, Hirosawa 2-1, Wako, Saitama 351-0198, Japan
[e] China Institute of Atomic Energy; Beijing, 102413, PR China
[f] Department of Physics, Kyoto University, Kita-shirakawa, Kyoto 606-8502, Japan
[g] Department of Physics, Korea University, Seoul 02841, Republic of Korea
[h] Institut für Kernphysik, Technische Universität Darmstadt, D-64289 Darmstadt, Germany
[i] GSI Helmholtzzentrum für Schwerionenforschung, Planckstrasse 1, 64291 Darmstadt, Germany
[j] Faculty of Physics, Astronomy and Applied Computer Science, Jagiellonian University, Kraków, Poland
[k] Division of Experimental Physics, Rudjer Boskovic Institute, Zagreb, Croatia
[l] Department of Physics, Rikkyo University, Nishi-Ikebukuro 3-34-1, Tokyo 171-8501, Japan
[m] Rare Isotope Science Project, Institute for Basic Science, Daejeon 34047, Republic of Korea
[n] Department of Physics, Tohoku University, Sendai 980-8578, Japan
[o] Department of Physics, Tokyo Institute of Technology, Tokyo 152-8551, Japan
[p] Institute of Nuclear Physics PAN, ul. Radzikowskiego 152, 31-342 Kraków, Poland
[q] Cyclotron Institute, Texas A&M University, College Station, TX 77843, USA
[r] Nikhef National Institute for Subatomic Physics, Amsterdam, Netherlands
[s] Department of Physics, Faculty of Science, King Mongkut's University of Technology Thonburi, Bangkok, Thailand
[t] Center of Excellence in Theoretical and Computational Science (TACS-CoE), Faculty of Science, King Mongkut's University of Technology Thonburi, Bangkok, Thailand
[u] Department of Physics, Tsinghua University, Beijing 100084, PR China
[v] Department of Chemistry, Texas A&M University, College Station, TX 77843, USA

ARTICLE INFO

Editor: Betram Blank

ABSTRACT

Properties of the nuclear equation of state (EoS) can be probed by measuring the dynamical properties of nucleus-nucleus collisions. In this study, we present the directed flow (v_1), elliptic flow (v_2) and stopping (VarXZ) measured in fixed target Sn + Sn collisions at 270 AMeV with the SπRIT Time Projection Chamber. We perform Bayesian analyses in which EoS parameters are varied simultaneously within the Improved Quantum Molecular Dynamics-Skyrme (ImQMD-Sky) transport code to obtain a multivariate correlated constraint. The

* Corresponding author at: Facility for Rare Isotope Beams, Michigan State University, East Lansing, MI 48824, USA.
** Corresponding author.
*** Corresponding author at: RIKEN Nishina Center, Hirosawa 2-1, Wako, Saitama 351-0198, Japan.
E-mail addresses: ctsang1@kent.edu (C.Y. Tsang), mizuki@riken.jp (M. Kurata-Nishimura), tsang@frib.msu.edu (M.B. Tsang), lynch@frib.msu.edu (W.G. Lynch), isobe@riken.jp (T. Isobe), murakami.tetsuya.3e@kyoto-u.jp (T. Murakami).

https://doi.org/10.1016/j.physletb.2024.138661
Received 17 April 2023; Received in revised form 19 February 2024; Accepted 16 April 2024
Available online 21 April 2024

varied parameters include symmetry energy, S_0, and slope of the symmetry energy, L, at saturation density, isoscalar effective mass, m_s^*/m_N, isovector effective mass, m_v^*/m_N and the in-medium cross-section enhancement factor η. We find that the flow and VarXZ observables are sensitive to the splitting of proton and neutron effective masses and the in-medium cross-section. Comparisons of ImQMD-Sky predictions to the SπRIT data suggest a narrow range of preferred values for m_s^*/m_N, m_v^*/m_N and η.

1. Introduction

Nuclear matter is a significant component of neutron stars, and understanding its properties can elucidate many features of these celestial objects. Calculating the properties of both nuclear matter and neutron stars requires extensive knowledge of the nuclear equation of state (EoS), which describes the dependence of nuclear-matter internal energy on various state variables. Progress in understanding nuclear EoS has been achieved through heavy ion collisions [1–3] and multimessenger astronomical observations of neutron stars [4–18]. In this paper, we present new experimental results on flow and stopping measurements from the SπRIT heavy ion collision experiment. Multiple observables are analyzed simultaneously using Bayesian inference to investigate correlations between various EoS parameters.

This paper is organized as follows: Section 2 provides a brief overview of the nuclear EoS and relevant parameters. This is followed by a discussion of the experimental setup and the selection of observables in Section 3. The transport model and Bayesian inference are discussed in Section 4. The experimental measurements and posterior constraints on EoS parameters are reported in Section 5, and finally, a summary is given in Section 6.

2. Nuclear equation of state

Nuclear EoS is a function of baryon number density ρ and asymmetry $\delta = (\rho_n - \rho_p)/\rho$, where δ represents the difference in neutron (ρ_n) and proton (ρ_p) number densities divided by total density ρ. We write the nuclear EoS as the sum of an isoscalar term $E_{\rm is}(\rho)$ and an isovector term $E_{\rm iv}(\rho,\delta)$, i.e. $E(\rho,\delta) = E_{\rm is}(\rho,\delta) + E_{\rm iv}(\rho,\delta)$. The first term, $E_{\rm is}(\rho)$, is the energy per nucleon of nuclear matter with equal proton and neutron densities ($\rho_p = \rho_n$); it provides the EoS of symmetric nuclear matter (SNM). The second term describes how the energy changes as a function of neutron-proton asymmetry. It can be approximately written as $E_{\rm iv}(\rho,\delta) = S(\rho)\delta^2 + \mathcal{O}(\delta^4)$, where $S(\rho)$ describes the dependence of nuclear EoS on neutron excess at different densities and is called the symmetry energy term. We truncate the expansion in δ at second order because the next (fourth) order term in δ contributes negligibly at asymmetries achieved in low energy nuclear collisions [19].

Many current heavy-ion collision efforts have focused on constraining the first few coefficients in a Taylor expansion of $S(\rho)$ around saturation density, $\rho_0 = 0.16\,\mathrm{fm}^{-3}$. Such expansions are commonly parameterized by,

$$S(\rho) = S_0 + Lx + \frac{1}{2}K_{\rm sym}x^2 + \mathcal{O}(x^3), \tag{1}$$

where $x = (\rho - \rho_0)/3\rho_0$ and S_0, L and $K_{\rm sym}$ are labels given to the first three expansion coefficients that describe the energy, slope and curvature of the EOS at saturation density, respectively. Similarly, the isoscalar term is commonly parameterized as,

$$E_{\rm is}(\rho) = E_0 + \frac{1}{2}K_0x^2 + \mathcal{O}(x^3), \tag{2}$$

where E_0 and K_0 are labels given to the first two non-zero expansion coefficients. From masses and other nuclide properties, the saturation energy for symmetric nuclear matter has been determined to be $E_0 = -15.8 \pm 0.5$ MeV [6]. Experiments that measured Giant Monopole resonances suggest that $K_0 = 230 \pm 30$ MeV [6].

Theoretical analysis has found that the form of momentum-dependent potential also affects $S(\rho)$ [20]. This momentum dependence can be quantified by ratios of the isoscalar effective mass, m_s^*, and isovector effective mass, m_v^*, to the mass of a nucleon, m_N, in free space. The isoscalar effective mass comes from the isoscalar part of the momentum dependent mean field potential [20]. In asymmetric matter, the strength of the neutron and proton effective mass splitting is related to the momentum dependence of the isovector mean-field potential. [21–23]. Near ρ_0, this splitting is related to the isovector effective mass $m_v^*/m_N = 1/(1+\kappa)$, where κ is the enhancement factor of the Thomas-Reiche-Kuhn sum rule [20,24].

The difference between the proton and neutron effective mass splitting, $\Delta m_{np}^*/\delta$, can be calculated from m_v^*/m_N and m_s^*/m_N with the following formula [25],

$$\frac{\Delta m_{np}^*}{\delta} \approx -2\left(\frac{m_N}{m_s^*} - \frac{m_N}{m_v^*}\right)\left(\frac{m_s^*}{m_N}\right)^2. \tag{3}$$

Recent measurements and analysis from the SπRIT experiment obtained a two-dimensional constraint on $\Delta m_{np}^*/\delta$ and L through pion spectral ratio [15]. The yield ratio of π^- to π^+ p_T spectra is used to derive this constraint because both $\Delta m_{np}^*/\delta$ and L influence the nucleon momenta; L quantifies the isospin dependent contribution to the nucleon potential energy and Δm_{np}^* quantifies the isospin dependent impact on the nucleon kinetic energy. Either increasing L or decreasing Δm_{np}^* will increase the energies of neutrons relative to protons. This increases the numbers of n-n collisions relative to p-p collisions at energies above the pion production threshold and enhances the production of π^- relative to that of π^+.

3. Experimental setup and observable selection

3.1. Experimental setup

The SπRIT experiment was performed at the Radioactive Isotope Beam Factory (RIBF), operated by RIKEN Nishina Center and Center for Nuclear Study, the University of Tokyo. In this experiment, we bombarded isotopically enriched ^{112}Sn and ^{124}Sn targets with secondary radioactive ^{108}Sn and ^{132}Sn beams and also stable ^{112}Sn and ^{124}S beams at 270 AMeV. The targets were placed at the entrance of the SπRIT Time Projection Chamber (TPC), which was installed inside the SAMURAI dipole magnet [26,27] at the RIBF. The SπRIT TPC identified and measured the momenta of charged particles [28,27,29,26] produced in ^{108}Sn+^{112}Sn, ^{112}Sn+^{124}Sn, ^{124}Sn+^{112}Sn and ^{132}Sn + ^{124}Sn collisions. Some results for the production of pions, hydrogen and helium isotopes have been previously published [30,15,31,32]. In this paper, we present analyses of collective flow and stopping from this experiment.

3.2. Observable selection

Collective flow is a descriptive label for a group of observables that have been widely used to constrain the nuclear EoS using heavy ion collisions [4,33–36,18,37]. It often involves analyses of anisotropies in the azimuthal distributions of emitted particles with respect to the reaction plane. Such collective flow observables in nucleus-nucleus collisions commonly reflect the pressures on *participant nucleons* in the overlapping region of projectile and target wherein this participant matter is compressed. Flow observables also reflect the presence of *spectator nucleons* that reside outside of the participant region and block the escape of participant nucleons from the compressed participant region.

Flow is a promising observable to constrain nuclear EoS because of its correlation with nuclear pressure. If the mean field is highly repulsive, participant nucleons experience higher pressures which leads to

early emission, but this emission is partially blocked by the spectator nucleons if they have not already moved past the participant region before it can expand into the spectator matter [4,38,39]. The blocking of the expanding participant matter by the spectator nucleons results in azimuthal anisotropies in fragment emissions. In very central collisions, there is very little spectator matter so emitted particles exhibit little anisotropies. With increasing impact parameter, the amount of spectator matter increases and the importance of the spectators blocking the emitted particles results in the increasing directional dependence that is characteristic of the directed flow.

Collective flow can be quantified by the Fourier coefficients of the fragments' azimuthal distributions with respect to the azimuthal angle for the reaction plane Φ [40],

$$\frac{dN}{d(\phi-\Phi)} \propto 1 + 2v_1\cos(\phi-\Phi) + 2v_2\cos(2(\phi-\Phi)) + \ldots \tag{4}$$

In the above equation, N is the particle yield, ϕ is the azimuthal angle of emission for the particle, v_1 is called the *directed flow* and v_2 is called the *elliptic flow*. Experimentally, v_1 and v_2 are calculated by the following formula,

$$\begin{aligned} v_1 &= \langle\cos(\phi-\Phi)\rangle, \\ v_2 &= \langle\cos(2(\phi-\Phi))\rangle. \end{aligned} \tag{5}$$

In this paper, we determined the azimuthal angle Φ of the reaction plane experimentally with the Q-vector method [41]. Q-vector is defined as,

$$\vec{Q} = \sum_{i=0}^{N} w_i \hat{p_{T}}_i \ \mathrm{sign}(y_{0i}), \tag{6}$$

where $\hat{p_{T}}_i$ is a unit vector pointing in the direction of the transverse momentum of the i^{th} track, $y_{0i} = (y_{CM}/y_{\mathrm{NN}})_i$ is the i^{th} particle's rapidity in the C.M. frame (y_{CM}) normalized by beam rapidity in the nucleon-nucleon frame ($y_{\mathrm{NN}} = 0.5y_{\mathrm{beamLab}}$), and sign($x$) is the sign function. We are free to choose the weighting factor w_i, with common choices including $w_i = 1$ or $w_i = p_T$. The effect of using different w_i will be considered as systematic uncertainty. The reaction plane angle Φ is chosen by the azimuthal angle of $\vec{Q}$. Although this approximation and the limited detector acceptance causes non-negligible broadening in the reaction plane resolution, appropriate formulas are used to correct for these effects. For details on these corrections, please refer to Ref. [41]. In this manuscript, we report only the flow values that have been corrected.

Equation (5) can be calculated by averaging over fragments of the same species. Both the theoretical and experimental values of v_1 and v_2 depend on the mass and species of each fragment, but the probability of producing a cluster of a particular mass depends on the details of the clusterization mechanism of each transport model. The underlying physics of this process is not accurately calculated by most transport codes [42,43], and this can result in significant systematic uncertainties in theoretical predictions of flow for different isotopes.

To compute light fragments, such as deuterons, tritons, and helium from final nucleon distribution from transport models, various cluster recognition methods have been employed, such as the minimum spanning tree method used in QMD type models [44]. This method classifies neutrons and protons that are emitted at small relative distances and momenta as heavy clusters. [44]. However, this process has a model dependence that reflects the influence of long-range multi-particle correlations that are not yet fully understood [42,43]. As a result, isotope-specific observable heavily depends on a detailed understanding of clusterization, and transport model predictions for these observables can often be unreliable.

To construct an observable that does not require an accurate description of the clusterization process, we calculate the *Coalescence Invariant flow* (C.I. flow) distributions. These distributions approximate the flow of nucleons prior to cluster formation by including contributions from p, d, t, ^{3}He and ^{4}He together in the calculation of averages of cosines in Eq. (5). Each fragment is weighted by their number of protons, i.e. Helium isotopes are weighted twice as much as Hydrogen isotopes. Fragments heavier than ^{4}He are not included due to their low yields.

Table 1
List of observables used in this analysis. The second column (Exp. $\langle b\rangle$) shows the averaged impact parameters of the selected experimental events in reconstruction of the observable.

Observable	Exp. $\langle b\rangle$	System
C.I. v_1 v.s. y_0	5.0 fm	^{108}Sn+^{112}Sn
	5.0 fm	^{132}Sn+^{124}Sn
C.I. v_1 v.s. p_T ($0.3 < y_0 < 0.8$)	5.0 fm	^{108}Sn+^{112}Sn
	5.0 fm	^{132}Sn+^{124}Sn
C.I. v_2 v.s. y_0	5.0 fm	^{108}Sn+^{112}Sn
	5.0 fm	^{132}Sn+^{124}Sn
VarXZ	1.0 fm	^{112}Sn+^{124}Sn

We select the impact parameter with gates on total detected charged particle multiplicity as described in Ref. [26]. This centrality selection method was also used in our previous SπRIT publications [30,15,31]. Due to the limited geometric acceptance in the SπRIT TPC, nuclear fragments with large momenta emitted at backward angles in the C.M. frame cannot be efficiently detected, so we limit our flow data to $0 \leq y_0 \leq 0.8$.

In addition to the mean field potentials in the EoS, momentum transfers that contribute to collective flow are also influenced by the in-medium nucleon-nucleon (NN) cross-section [45,46]. We construct the stopping observable, $VarXZ = VarX/VarZ$, where $VarX$ and $VarZ$ are the variances of particle rapidity distributions in the transverse and longitudinal directions, respectively. Since VarXZ is a ratio of variances, much of the systematic error from clusterization is cancelled out in the division. VarXZ measures the degree of stopping and thermalization [47], and has also been used to probe the nuclear shear viscosity [48]. It is closely influenced by the in-medium cross-section [47].

To reconstruct this observable and calculate the momentum of the particles accurately, only tracks emitted nearly perpendicular to the magnetic field of the TPC are used. Based on the performance of the SπRIT TPC [49], azimuth cuts of $330° < \phi < 360°$, $0° < \phi < 20°$ and $160° < \phi < 210°$ are used for this purpose. These cuts are also used in the other SπRIT analyses [30,15,50,32]. Since determination of the reaction plane does not require as precise values for the magnitude of the momenta of particles, and to minimize bias due to particle cut, we do not impose these restrictive cuts in azimuthal angle on particles in calculating azimuthal orientation of the reaction plane.

The x-axis in $VarX$ can be any arbitrary laboratory axis that is perpendicular to the beam axis, consistent with definitions in Ref. [47]. Given the arbitrary azimuthal orientation of the x-axis for the $VarX$ observable, we can and do calculate x-rapidity distribution by projecting p_T of each track onto planes with random azimuthal angles.

SπRIT TPC cannot efficiently measure fragments at $y_0 < 0$ so data is not available at all rapidities for ^{108}Sn+^{112}Sn and ^{132}Sn+^{124}Sn reactions, individually. However, we have constructed the full rapidity distribution of ^{112}Sn+^{124}Sn by combining the results of ^{112}Sn+^{124}Sn and ^{124}Sn+^{112}Sn reactions. Our evaluation of VarXZ is limited only to this reaction system as the other systems do not have the corresponding mirror reactions. In the following, we select central events of $\langle b\rangle = 1$ fm in order to maximize contributions from nucleon-nucleon collisions. The absence of the flow analysis from ^{112}Sn+^{124}Sn should impact our conclusion minimally since the δ value of ^{112}Sn+^{124}Sn is between that of ^{108}Sn+^{112}Sn and ^{132}Sn+^{124}Sn systems, therefore the range of asymmetry being studied is not affected.

Table 1 summarizes all observables for the corresponding reactions that will be used in this manuscript for comparison with models. Frag-

ments at mid-rapidity have small v_1, so the rapidity range of v_1 when being plotted as a function of p_T is narrowed down to $0.3 < y_0 < 0.8$ to enhance the sensitivity. Their average impact parameters selected from multiplicity gates are shown in the second column and the corresponding reaction systems are shown in the third.

3.3. Observable uncertainties

Three independent sources of systematic uncertainties are considered in the reconstruction of C.I. flow: 1) the variation of the Q-vector weighting conditions, 2) the variation of track selection and 3) variation of impact parameter selection. To quantify the uncertainty due to the variation in the Q-vector weights w_i, we reconstruct each flow spectrum multiple times using different forms of w_i for Q-vector calculation. Next, we fix the weights in the Q-vector and vary the goodness of track selection conditions to estimate the systematic uncertainty from the second source, which includes varying the minimal track length threshold and azimuth cuts. Finally, we reconstruct the observable with a different multiplicity gate. The upper and lower limits of the multiplicity gate are varied in such a way that the average impact parameter remains unchanged. We determine the systematic uncertainty as the bin-by-bin difference between spectra constructed using the default and varied multiplicity gate.

For VarXZ, systematic uncertainty is considered by varying track and impact parameter selection. The total observable uncertainty for both VarXZ and flow is obtained by adding the statistical uncertainty and all sources of systematic uncertainties in quadrature. The experimental values and uncertainties are presented in Appendix A.

4. Transport model and Bayesian inference

All measurements in Table 1 are compared simultaneously to predictions from the Improved Quantum Molecular Dynamic-Skyrme model (ImQMD-Sky) [51,52], which has been frequently used to study nucleus-nucleus collisions at similar beam energies [14]. In the model, the nucleonic potential energy density without the spin-orbit term is given by the sum of two terms, $u_{\rm loc} + u_{\rm md}$, where,

$$u_{\rm loc} = \frac{\alpha}{2}\frac{\rho^2}{\rho_0} + \frac{\beta}{\gamma+1}\frac{\rho^{\gamma+1}}{\rho_0^{\gamma}} + \frac{g_{\rm sur}}{2\rho_0}(\nabla\rho)^2 + \frac{g_{\rm sur,iso}}{\rho_0}[\nabla(\rho_n-\rho_p)]^2 + A_{\rm sym}\frac{\rho^2}{\rho_0}\delta^2 + B_{\rm sym}\frac{\rho^{\gamma+1}}{\rho_0^{\gamma}}\delta^2. \tag{7}$$

Parameters will be defined in the next paragraph. The Skyrme-type momentum-dependent energy density functional, $u_{\rm md}$ stems from an interaction of the form $\delta(\mathbf{r}_1-\mathbf{r}_2)(\mathbf{p}_1-\mathbf{p}_2)^2$ [53,54,52] and is written as,

$$u_{\rm md} = C_0\sum_{ij}\int d^3p d^3p' f_i(\mathbf{r},\mathbf{p}) f_j(\mathbf{r},\mathbf{p}')(\mathbf{p}-\mathbf{p}')^2 + D_0\sum_{ij\in {\rm n}}\int d^3p d^3p' f_i(\mathbf{r},\mathbf{p}) f_j(\mathbf{r},\mathbf{p}')(\mathbf{p}-\mathbf{p}')^2 + D_0\sum_{ij\in {\rm p}}\int d^3p d^3p' f_i(\mathbf{r},\mathbf{p}) f_j(\mathbf{r},\mathbf{p}')(\mathbf{p}-\mathbf{p}')^2. \tag{8}$$

There are nine parameters in Equations (7) and (8), which are α, β, γ, $A_{\rm sym}$, $B_{\rm sym}$, C_0, D_0, $g_{\rm sur}$ and $g_{\rm sur,iso}$. Calculations show that the predicted observables are relatively insensitive to $g_{\rm sur}$ and $g_{\rm sur,iso}$ [20]. We therefore set them to $g_{\rm sur} = 24.5\,{\rm MeV\,fm^2}$ and $g_{\rm sur,iso} = -4.99\,{\rm MeV\,fm^2}$. These parameters are the same as those derived from the commonly used Skyrme interaction SLy4 [55].

The remaining seven free parameters are related to the seven nuclear EoS parameters (ρ_0, $E_{\rm sat}$, $K_{\rm sat}$, S_0, L, m_s^* and m_v^*) through appropriate formulas from Refs. [56,57]. The saturation density and coefficients of isoscalar terms are well constrained from previous studies, so they are fixed to $\rho_0 = 0.155\,{\rm fm^{-3}}$, $E_0 = -15.8\,{\rm MeV}$ and $K_0 = 230\,{\rm MeV}$ [6]. The four remaining EoS parameters (S_0, L, m_s^*/m_N and m_v^*/m_N) and the in-medium cross-section enhancement factor η (defined in the next paragraph) are varied in this study.

In ImQMD-Sky, the in-medium NN cross section is formulated in a phenomenological form,

$$\sigma_{\rm QMD}^{\rm med} = \left(1 - \frac{\eta\rho}{\rho_0}\right)\sigma^{\rm free}, \tag{9}$$

where $\sigma^{\rm free}$ is the NN cross-section in free space from Ref. [58] and η is the enhancement factor to be determined. Note that with this definition, η has the opposite sign than what was used previously in Ref. [45]. In Eq. (9), positive η implies that the in-medium cross section is reduced from that for free nucleon-nucleon scattering.

Bayesian inference is performed to convert experimental results into correlated constraints on all five varying parameters. This analysis requires *prior* distributions as input, which encodes our initial belief in parameter values from previous studies. The analysis returns a multivariate distribution called the *posterior*, which is the probability distribution of parameter values conditioned on the measured observables using the Bayes theorem. Let $\vec{x}$ be the list of parameters and $\vec{O}$ be the list of measured observable values. Bayes theorem then states that,

$$P(\vec{x}|\vec{O}) \propto P(\vec{x})P(\vec{O}|\vec{x}). \tag{10}$$

In this equation, $P(\vec{x}|\vec{O})$ is the posterior, $P(\vec{x})$ is the prior and $P(\vec{O}|\vec{x})$ is called the *likelihood*, which is the probability of getting the observed results provided that parameter values in set $\vec{x}$ are the true values. Likelihood is usually modelled as,

$$P(\vec{O}|\vec{x}) \propto \exp\left(-\frac{1}{2}(\vec{O}-\vec{O}^{\rm model}(\vec{x}))\Sigma^{-1}(\vec{O}-\vec{O}^{\rm model}(\vec{x}))^T\right), \tag{11}$$

where $\vec{O}$ is the list of all measured observables arranged as a vector, $\vec{O}^{\rm model}(\vec{x})$ is the predicted values from theoretical model for a given parameter set $\vec{x}$ and $\Sigma = \Sigma(\vec{O}^{\rm model}) + {\rm diag}(\sigma_O)$ is the combined covariance matrix for theoretical and experimental uncertainties, with the first term $\Sigma(\vec{O}^{\rm model})$ denoting the covariance matrix of all model predictions and ${\rm diag}(\sigma_O)$ is a diagonal matrix with experimental uncertainty as the diagonal values.

In this work, Markov chain Monte Carlo (MCMC) from the PyMC2 package [59] is used to compute the posterior distribution. To speed up the MCMC process, we employ Gaussian emulators [60] and Principal Component Analysis to efficiently interpolate predictions from ImQMD-Sky on just 70 parameter sets and estimate model covariance $\Sigma(\vec{O}^{\rm model})$. Two Principal Components are used for each observable, capturing more than 95% of the variance in all the training spectrum. These parameter sets are sampled uniformly and randomly on a Latin hypercube within the parameter ranges given in Table 2. The ranges of L, m_s^*/m_N and m_v^*/m_N are maximal, meaning that beyond these ranges ImQMD-Sky is unable to simulate correctly. For each parameter set and system in Table 1, the training spectrum are generated from 20,000 ImQMD-Sky simulated collisions. The simulation time of ImQMD-Sky is 400 fm/c, long after the time when the collision dynamics finishes and the observables reach their asymptotic values. We have verified that our observables reach their asymptotic values when the simulation time is greater than 300 fm/c. The final MCMC posterior is generated with 630,000 iterations.

When five parameter sets are removed from interpolation, the interpolation error does not increase, which indicates that 70 sets are more than sufficient. Gaussian priors of $S_0 \sim {\rm Gaus}(\mu = 35.3, \sigma = 2.8)$ MeV and $L \sim {\rm Gaus}(\mu = 80, \sigma = 38)$ MeV are used while uniform priors within the experimental known ranges are used for the effective masses and η. The priors on S_0 and L come from the posterior distributions from the analysis of pion spectral ratios in the same experiment [15].

ImQMD-Sky calculations are done at $b = 5$ fm for flow observables and $b = 1$ fm for stopping observables. They are chosen to match the

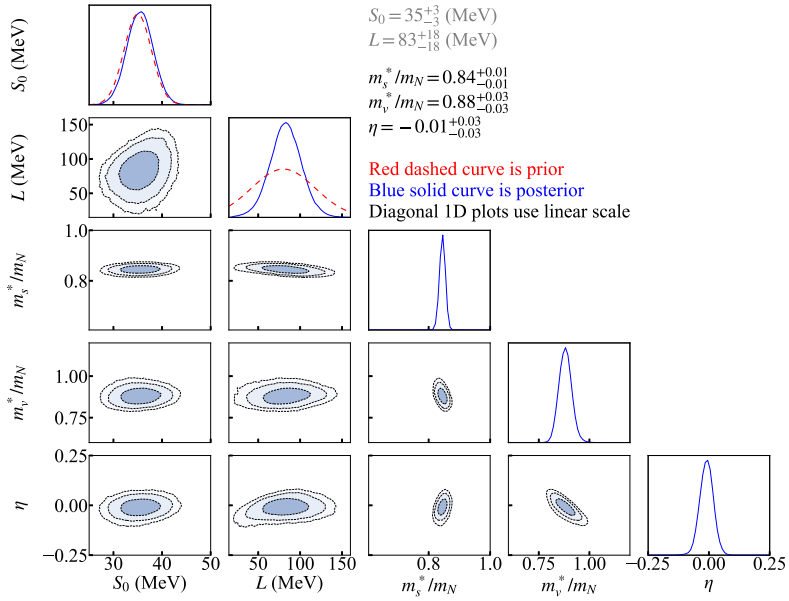

Fig. 1. Posterior distribution after ImQMD-Sky's predictions is compared to experimental data with Bayesian analysis using MCMC. The median and 68% confidence interval of the parameters are listed on the upper right hand side of the figure. The numbers for S_0 and L are grayed out to signify their dependence on prior. See text for details. Priors of S_0 and L are plotted on the diagonal plot as red dashed curves, and the priors of the other parameters are all uniform so they are not plotted for clarity. The outer boundaries for the three shaded blue regions in the off-diagonal plots, from the deepest to the lightest shades of blue, correspond to the 68%, 95% and 99% confidence intervals, respectively.

Table 2
The ranges of parameters for Bayesian analysis. The last two columns show the Gaussian prior mean and standard deviation (σ) for S_0 and L. The last three parameters have uniform prior so no numbers are provided.

Parameters	Min.	Max.	Mean	σ
S_0 (MeV)	25	52	35.3	2.8
L (MeV)	18	160	80	38
m_s^*/m_N	0.6	1	Uniform	
m_v^*/m_N	0.6	1.2	Uniform	
η	-0.3	0.3	Uniform	

mean impact parameters of the observables in Table 1. Note that the range of possible impact parameters that contribute to the experimental measurements actually varies due to multiplicity fluctuations. Ideally, we should simulate events with a realistic distribution of impact parameters and apply the same multiplicity cut as data. Unfortunately, the multiplicity distributions of most transport models are not precisely comparable to data due to issues with coalescence algorithms described in Section 3.2.

5. Analysis results

The posterior is shown in Fig. 1. Despite employing uniform priors, tight constraints on m_s^*/m_N, m_v^*/m_N and η are observed. These constraints are robust constraints as they do not show a significant correlation with either S_0 or L, indicating that their posterior values remain unaffected by our choice of prior.

In contrast, the posterior distributions of S_0 and L are wide even when Gaussian priors are used. The posterior distribution of S_0 looks very similar to the prior, indicating that our choice of observables lacks sensitivity to S_0. Although there is a modest improvement in the constraint on L compared to the prior distribution, Fig. 1 also highlights a correlation between S_0 and L. Consequently, the marginalized value of L (83 ± 18 MeV) may change if a different prior for S_0 is employed.

The near-zero value of $\eta = -0.01^{+0.03}_{-0.03}$ indicates that the in-medium cross-section is similar to the free cross-section. This differs from previous analyses performed at different beam energies, where an enhancement in the in-medium cross-section is derived [45]. Our results contrast with those of Ref. [46], which reported a reduction in in-medium cross-section using UrQMD and Au + Au data from FOPI. Unlike their study, where the in-medium cross-section was the sole parameter varied, our global fit involved simultaneous adjustments to five parameters. Furthermore, our analysis considered coalescence invariant flow, while Ref. [46] relied on flow results for free protons. The observed disparities may be attributed to potential afterburner effects on in-medium cross-section outcomes.

Fig. 2 shows the fitted flow and stopping observables. The first three rows show the results of directed and elliptic flow, with plots on the left column corresponding to the results of ^{108}Sn+^{112}Sn reaction and the right ^{132}Sn+^{124}Sn. From top to bottom, the three rows show v_1 as a function of y_0, v_1 as a function of p_T (MeV) and v_2 as a function of y_0, all at $\langle b \rangle = 5$ fm. The fourth row shows VarXZ for ^{112}Sn+^{124}Sn at $\langle b \rangle = 1$ fm.

To test the prediction power of our results, our most probable values of $S_0 = 35$ MeV, $L = 83$ MeV, $m_s^*/m_N = 0.84$, $m_v^*/m_N = 0.88$ and $\eta = -0.01$ are used to predict VarXZ of protons, deuterons and tritons for ^{197}Au + ^{197}Au and ^{129}Xe + ^{133}Cs at a fixed-target beam energy of 250 AMeV with the ImQMD-Sky model. VarXZs from these two systems are chosen because their values were measured experimentally in Ref. [47]. Experimental values of VarXZs at other beam energies are also available, but the beam energy at 250 AMeV is the closest to the SπRIT beam energy of 270 AMeV. Our choice minimizes effects due to changing beam energy and isolates the dependence on system size. Predictions from ImQMD-Sky are plotted on top of experimental values in Fig. 3 which shows reasonable agreement with an exception of proton from Au + Au at 250 AMeV, where less stopping is observed than the model prediction. It is a good indication that our results are applicable to collisions of various system sizes near 270 AMeV.

The posterior on effective masses can be converted to a probability distribution on effective mass splitting $\Delta m_{np}^*/\delta$ using Eq. (3) and we find that $\Delta m_{np}^*/\delta = -0.07^{+0.07}_{-0.06}$. The value of effective mass splitting differs among various analyses using different data, but most of them favor

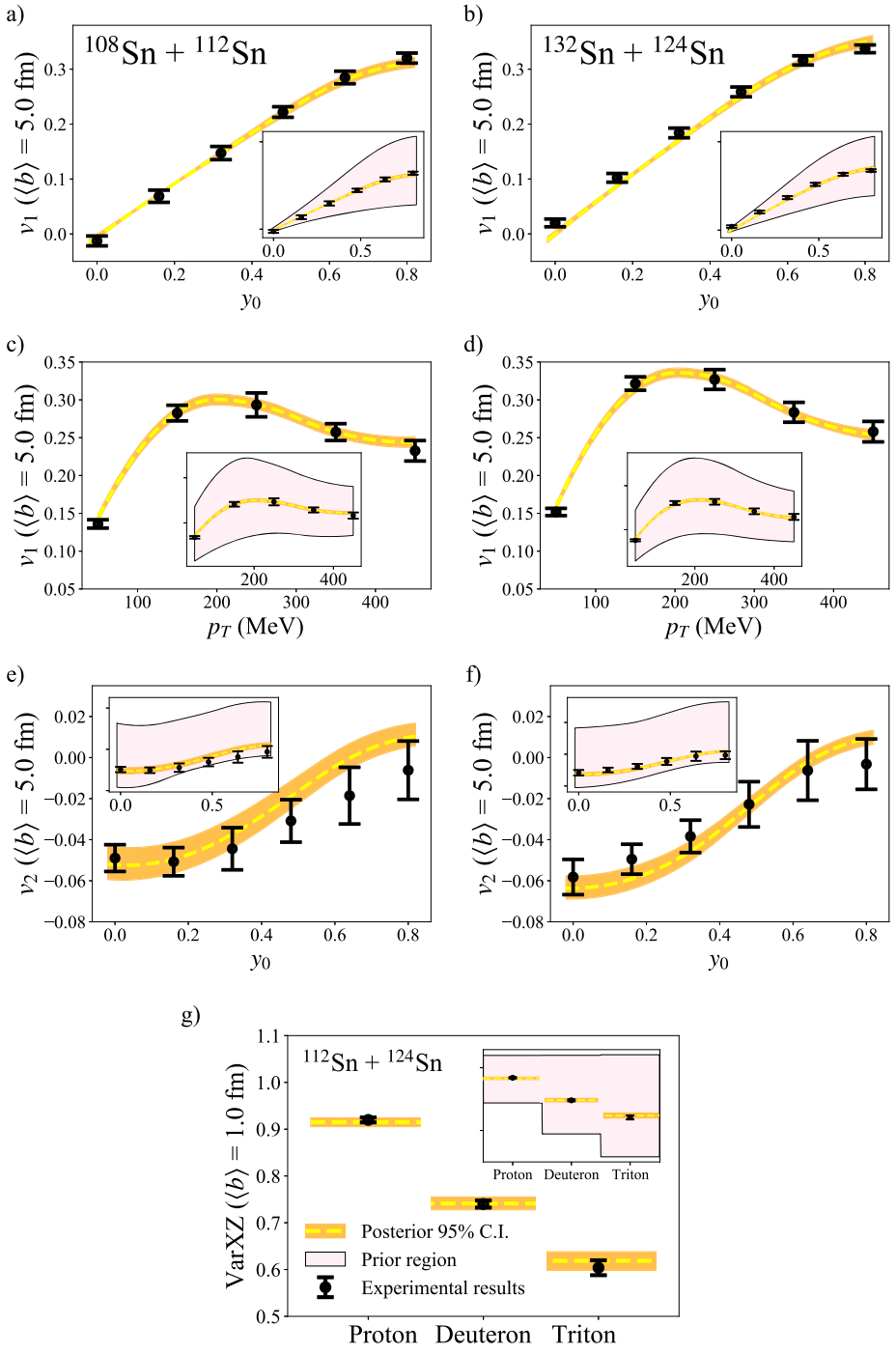

Fig. 2. This figure compares directed (a, b, c, d), elliptic flow (e, f) and VarXZ (g) between the best fitted ImQMD-Sky predictions and experimental results. The black points show results from SπRIT experiment. The orange region shows the 2σ confidence region of ImQMD-Sky prediction from posterior distribution. The small sub-figure in each figure also shows a wide pink region that corresponds to the maximum ranges of prediction values from ImQMD-Sky with the parameter range in Table 2. (a, c, e) show results for ^{108}Sn+ ^{112}Sn and (b, d, f) show results for ^{132}Sn+ ^{124}Sn. (g) shows the stopping results for ^{112}Sn+ ^{124}Sn.

a positive value [61]. Of all the analyses in Ref. [61], the only result that favors a negative value of $\Delta m^*_{np}/\delta$ comes from the study of the n/p ratio from heavy ion reactions which yields $\delta m^*_{np}/\delta = -0.05 \pm 0.09$ [14]. That analysis also uses the ImQMD-Sky model for inference. It may indicate that the momentum dependence of the isovector mean fields in the ImQMD-Sky transport theory prefers a lower value of effective mass splitting.

Similar to constraints from pion observables [15], we observed a correlation from this analysis between $\Delta m^*_{np}/\delta$ and L, as Fig. 4 demonstrates. The correlation trends in Ref. [15] are nearly orthogonal to the present work. While ImQMD-Sky is used for the current constraint, dcQMD was used in the pion analysis. Clearly, the model dependence of effective mass and symmetry energy effects must be studied carefully, ideally within an effort like the Transport Model Evaluation Project (TMEP) [62]. Such endeavors will deepen our understanding of model dependence of EoS parameters and hopefully develop ways for constraints from different models to be compared and combined reliably. Even though a direct comparison is not feasible right now, this study opens an opportunity to improve constraints on L by combining Fig. 4 with correlated constraints between L and $\Delta m^*_{np}/\delta$ from Ref. [15].

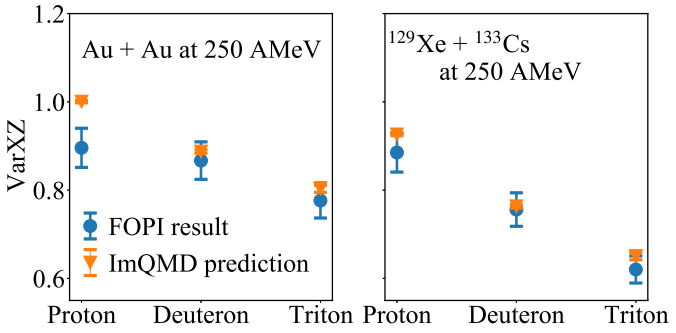

Fig. 3. VarXZ of proton, deuteron and triton for ^{197}Au + ^{197}Au and ^{129}Xe + ^{133}Cs reactions at 250 AMeV at $b = 1$ fm. The orange inverted triangles show ImQMD-Sky predictions using the best fitted parameter values obtained from the SπRIT experiment. The blue circles show experimental results from the FOPI data set.

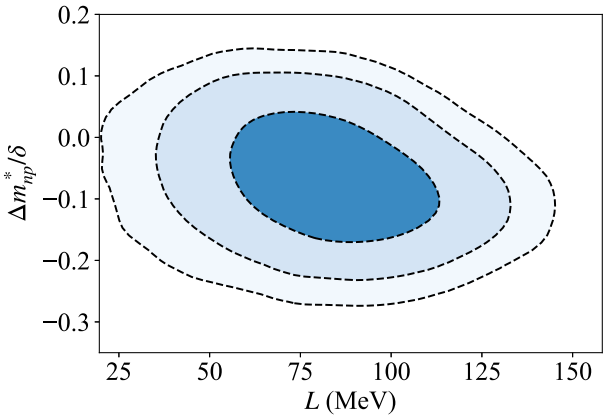

Fig. 4. Correlation between L and $\Delta m^*_{np}/\delta$. The three shades of blue, from the deepest to the lightest, correspond to 68%, 95% and 99% confidence intervals.

6. Summary and conclusion

Directed flow (v_1) and elliptic flow (v_2) of ^{108}Sn+^{112}Sn and ^{132}Sn+^{124}Sn and stopping (VarXZ) of ^{112}Sn+^{124}Sn (all at fixed-target beam energy of 270 AMeV) are extracted from the data obtained in the SπRIT experiment. The measured values are compared to predictions from the Improved Quantum Molecular Dynamic-Skyrme (ImQMD-Sky) model through a Bayesian analysis which shows strong constraining power on the effective masses (m^*_s/m_N and m^*_v/m_N) and the in-medium cross-section parameter (η). The most probable values are $m^*_s/m_N = 0.84 \pm 0.01$, $m^*_v/m_N = 0.88 \pm 0.03$, and $\eta = -0.01 \pm 0.03$. The constraints on effective mass are converted to a probability distribution on effective mass splitting to give $\Delta m^*_{np}/\delta = -0.07^{+0.07}_{-0.06}$. This can be used to tighten constraints on symmetry energy terms such as L as it was demonstrated to be correlated to $\Delta m^*_{np}/\delta$, but efforts in understanding model dependence of analysis on nucleon effective masses are warranted for the comparison to be conclusive. As studies on effective mass deepen, our findings could serve as a benchmark for the development of future transport models.

Declaration of competing interest

The authors declare that they have no known competing financial interests or personal relationships that could have appeared to influence the work reported in this paper.

Data availability

Experimental data is tabulated on the manuscript.

Acknowledgements

The authors would like to thank members of the Transport Model Evaluation Project collaboration for many fruitful discussions. This work was supported by U.S. National Science Foundation Grant No. PHY-2209145, Department of Energy Grant No. DE-FG02-93ER40773, Department of Energy National Nuclear Security Administration Stewardship Science Graduate Fellowship under cooperative Agreement No. DE-NA0002135, The Robert A. Welch Foundation (A-1266 and A-1358), the Japanese MEXT KAKENHI (Grant-in-Aid for Scientific Research on Innovative Areas) grant No. 24105004, JSPS KAKENHI Grants Nos. JP17K05432, JP19K14709 and JP21K03528, the National Research Foundation of Korea under grant Nos. 2018R1A5A1025563 and 2013M7A1A1075764, the Polish National Science Center (NCN) under contract Nos. UMO-2013/09/B/ST2/04064, UMO-2013/-10/M/ST2/00624, the Ministry of Science and Technology of China under grant Nos. 2022YFE0103400 and Tsinghua University Initiative Scientific Research Program. Computing resources were provided by Facility for Rare Isotope Beams (FRIB), the HOKUSAI-Great Wave system at RIKEN under grants Nos. G17033,Q18-23393, supported by Pioneering Program of RIKEN for Evolution of Matter in the Universe (r-EMU) and the Institute for Cyber-Enabled Research at Michigan State University.

Appendix A. SπRIT data

All experimental data and uncertainties are tabulated in Table A.1.

Table A.1
Experimental values and the associated statistical and systematic uncertainties.

(a) v_1 as a function of y_0 for ^{108}Sn+^{112}Sn at $\langle b \rangle = 5$ fm.

y_0	0.000	0.160	0.320	0.480	0.640	0.800
v_1	-0.013	0.069	0.147	0.222	0.285	0.320
Stat.	0.002	0.002	0.002	0.002	0.002	0.002
Sys.	0.009	0.011	0.012	0.009	0.011	0.009

(b) v_1 as a function of y_0 for ^{132}Sn+^{124}Sn at $\langle b \rangle = 5$ fm.

y_0	0.000	0.160	0.320	0.480	0.640	0.800
v_1	0.020	0.102	0.184	0.259	0.316	0.337
Stat	0.002	0.002	0.002	0.002	0.002	0.002
Sys	0.007	0.008	0.009	0.009	0.008	0.007

(c) v_1 as a function of p_T (MeV/c) for ^{108}Sn+^{112}Sn at $\langle b \rangle = 5$ fm.

p_T	50	150	250	350	450
v_1	0.136	0.283	0.293	0.257	0.233
Stat.	0.002	0.002	0.002	0.003	0.004
Sys.	0.005	0.010	0.016	0.011	0.013

(d) v_1 as a function of p_T (MeV/c) for ^{132}Sn+^{124}Sn at $\langle b \rangle = 5$ fm.

p_T	50	150	250	350	450
v_1	0.152	0.322	0.327	0.284	0.258
Stat	0.002	0.002	0.002	0.003	0.004
Sys	0.004	0.009	0.013	0.013	0.013

(e) v_2 as a function of y_0 for ^{108}Sn+^{112}Sn at $\langle b \rangle = 5$ fm.

y_0	0.000	0.160	0.320	0.480	0.640	0.800
v_2	-0.049	-0.051	-0.044	-0.031	-0.019	-0.006
Stat.	0.003	0.003	0.003	0.003	0.003	0.003
Sys.	0.006	0.006	0.010	0.010	0.013	0.014

(f) v_2 as a function of y_0 for ^{132}Sn+^{124}Sn at $\langle b \rangle = 5$ fm.

y_0	0.000	0.160	0.320	0.480	0.640	0.800
v_2	-0.058	-0.049	-0.038	-0.023	-0.006	-0.003
Stat.	0.003	0.003	0.003	0.003	0.003	0.003
Sys.	0.008	0.007	0.007	0.011	0.014	0.012

(g) VarXZ of proton, deuteron and triton for ^{112}Sn+^{124}Sn at $\langle b \rangle = 1$ fm.

y_0	proton	deuteron	triton
VarXZ	0.915	0.767	0.590
Stat.	0.004	0.005	0.003
Sys.	0.011	0.012	0.010

References

[1] J. Xu, Transport approaches for the description of intermediate-energy heavy-ion collisions, Prog. Part. Nucl. Phys. 106 (2019) 312–359, https://doi.org/10.1016/j.ppnp.2019.02.009.

[2] A. Sorensen, K. Agarwal, K.W. Brown, Z. Chajecki, P. Danielewicz, C. Drischler, S. Gandolfi, J.W. Holt, M. Kaminski, C.-M. Ko, R. Kumar, B.-A. Li, W.G. Lynch, A.B. McIntosh, W.G. Newton, S. Pratt, O. Savchuk, M. Stefaniak, I. Tews, M.B. Tsang, R. Vogt, H. Wolter, H. Zbroszczyk, N. Abbasi, J. Aichelin, A. Andronic, S.A. Bass, F. Becattini, D. Blaschke, M. Bleicher, C. Blume, E. Bratkovskaya, B.A. Brown, D.A. Brown, A. Camaiani, G. Casini, K. Chatziioannou, A. Chbihi, M. Colonna, M.D. Cozma, V. Dexheimer, X. Dong, T. Dore, L. Du, J.A. Dueñas, H. Elfner, W. Florkowski, Y. Fujimoto, R.J. Furnstahl, A. Gade, T. Galatyuk, C. Gale, F. Geurts, S. Grozdanov, K. Hagel, S.P. Harris, W. Haxton, U. Heinz, M.P. Heller, O. Hen, H. Hergert, N. Herrmann, H.Z. Huang, X.-G. Huang, N. Ikeno, G. Inghirami, J. Jankowski, J. Jia, J.C. Jiménez, J. Kapusta, B. Kardan, I. Karpenko, D. Keane, D. Kharzeev, A. Kugler, A.L. Fèvre, D. Lee, H. Liu, M.A. Lisa, W.J. Llope, I. Lombardo, M. Lorenz, T. Marchi, L. McLerran, U. Mosel, A. Motornenko, B. Müller, P. Napolitani, J.B. Natowitz, W. Nazarewicz, J. Noronha, J. Noronha-Hostler, G. Odyniec, P. Papakonstantinou, Z. Paulínyová, J. Piekarewicz, R.D. Pisarski, C. Plumberg, M. Prakash, J. Randrup, C. Ratti, P. Rau, S. Reddy, H.-R. Schmidt, P. Russotto, R. Ryblewski, A. Schäfer, B. Schenke, S. Sen, P. Senger, R. Seto, C. Shen, B. Sherrill, M. Singh, V. Skokov, M. Spaliński, J. Steinheimer, M. Stephanov, J. Stroth, C. Sturm, K.-J. Sun, A. Tang, G. Torrieri, W. Trautmann, G. Verde, V. Vovchenko, R. Wada, F. Wang, G. Wang, K. Werner, N. Xu, Z. Xu, H.-U. Yee, S. Yennello, Y. Yin, Dense nuclear matter equation of state from heavy-ion collisions, arXiv:2301.13253, 2023.

[3] W. Lynch, M. Tsang, Decoding the density dependence of the nuclear symmetry energy, Phys. Lett. B 830 (2022) 137098, https://doi.org/10.1016/j.physletb.2022.137098.

[4] P. Danielewicz, R. Lacey, W.G. Lynch, Determination of the equation of state of dense matter, Science 298 (5598) (2002) 1592–1596, https://doi.org/10.1126/science.1078070.

[5] A.L. Fèvre, Y. Leifels, W. Reisdorf, J. Aichelin, C. Hartnack, Constraining the nuclear matter equation of state around twice saturation density, Nucl. Phys. A 945 (2016) 112–133, https://doi.org/10.1016/j.nuclphysa.2015.09.015.

[6] M. Dutra, O. Lourenço, J.S. Sá Martins, A. Delfino, J.R. Stone, P.D. Stevenson, Skyrme interaction and nuclear matter constraints, Phys. Rev. C 85 (2012) 035201, https://doi.org/10.1103/PhysRevC.85.035201.

[7] Z. Zhang, L.-W. Chen, Electric dipole polarizability in ^{208}Pb as a probe of the symmetry energy and neutron matter around $\rho_0/3$, Phys. Rev. C 92 (3) (2015) 031301.

[8] D. Adhikari, H. Albataineh, D. Androic, K. Aniol, D.S. Armstrong, T. Averett, C. Ayerbe Gayoso, S. Barcus, V. Bellini, R.S. Beminiwattha, J.F. Benesch, H. Bhatt, D. Bhatta Pathak, D. Bhetuwal, B. Blaikie, Q. Campagna, A. Camsonne, G.D. Cates, Y. Chen, C. Clarke, J.C. Cornejo, S. Covrig Dusa, P. Datta, A. Deshpande, D. Dutta, C. Feldman, E. Fuchey, C. Gal, D. Gaskell, T. Gautam, M. Gericke, C. Ghosh, I. Halilovic, J.-O. Hansen, F. Hauenstein, W. Henry, C.J. Horowitz, C. Jantzi, S. Jian, S. Johnston, D.C. Jones, B. Karki, S. Katugampola, C. Keppel, P.M. King, D.E. King, M. Knauss, K.S. Kumar, T. Kutz, N. Lashley-Colthirst, G. Leverick, H. Liu, N. Liyange, S. Malace, R. Mammei, J. Mammei, M. McCaughan, D. McNulty, D. Meekins, C. Metts, R. Michaels, M.M. Mondal, J. Napolitano, A. Narayan, D. Nikolaev, M.N.H. Rashad, V. Owen, C. Palatchi, J. Pan, B. Pandey, S. Park, K.D. Paschke, M. Petrusky, M.L. Pitt, S. Premathilake, A.J.R. Puckett, B. Quinn, R. Radloff, S. Rahman, A. Rathnayake, B.T. Reed, P.E. Reimer, R. Richards, S. Riordan, Y. Roblin, S. Seeds, A. Shahinyan, P. Souder, L. Tang, M. Thiel, Y. Tian, G.M. Urciuoli, E.W. Wertz, B. Wojtsekhowski, B. Yale, T. Ye, A. Yoon, A. Zec, W. Zhang, J. Zhang, X. Zheng, Accurate determination of the neutron skin thickness of ^{208}Pb through parity-violation in electron scattering, Phys. Rev. Lett. 126 (2021) 172502, https://doi.org/10.1103/PhysRevLett.126.172502.

[9] B.T. Reed, F.J. Fattoyev, C.J. Horowitz, J. Piekarewicz, Implications of PREX-2 on the equation of state of neutron-rich matter, Phys. Rev. Lett. 126 (17) (2021) 172503.

[10] B.A. Brown, Constraints on the Skyrme equations of state from properties of doubly magic nuclei, Phys. Rev. Lett. 111 (2013) 232502, https://doi.org/10.1103/PhysRevLett.111.232502.

[11] M. Kortelainen, J. McDonnell, W. Nazarewicz, P.-G. Reinhard, J. Sarich, N. Schunck, M.V. Stoitsov, S.M. Wild, Nuclear energy density optimization: large deformations, Phys. Rev. C 85 (2) (2012) 024304.

[12] P. Danielewicz, P. Singh, J. Lee, Symmetry energy III: isovector skins, Nucl. Phys. A 958 (2017) 147–186, https://doi.org/10.1016/j.nuclphysa.2016.11.008, arXiv:1611.01871.

[13] M.B. Tsang, Y. Zhang, P. Danielewicz, M. Famiano, Z. Li, W.G. Lynch, A.W. Steiner, Constraints on the density dependence of the symmetry energy, Phys. Rev. Lett. 102 (2009) 122701, https://doi.org/10.1103/PhysRevLett.102.122701.

[14] P. Morfouace, C. Tsang, Y. Zhang, W. Lynch, M. Tsang, D. Coupland, M. Youngs, Z. Chajecki, M. Famiano, T. Ghosh, G. Jhang, J. Lee, H. Liu, A. Sanetullaev, R. Showalter, J. Winkelbauer, Constraining the symmetry energy with heavy-ion collisions and Bayesian analyses, Phys. Lett. B 799 (2019) 135045, https://doi.org/10.1016/j.physletb.2019.135045.

[15] J. Estee, W.G. Lynch, C.Y. Tsang, J. Barney, G. Jhang, M.B. Tsang, R. Wang, M. Kaneko, J.W. Lee, T. Isobe, M. Kurata-Nishimura, T. Murakami, D.S. Ahn, L. Atar, T. Aumann, H. Baba, K. Boretzky, J. Brzychczyk, G. Cerizza, N. Chiga, N. Fukuda, I. Gasparic, B. Hong, A. Horvat, K. Ieki, N. Inabe, Y.J. Kim, T. Kobayashi, Y. Kondo, P. Lasko, H.S. Lee, Y. Leifels, J. Łukasik, J. Manfredi, A.B. McIntosh, P. Morfouace, T. Nakamura, N. Nakatsuka, S. Nishimura, H. Otsu, P. Pawłowski, K. Pelczar, D. Rossi, H. Sakurai, C. Santamaria, H. Sato, H. Scheit, R. Shane, Y. Shimizu, H. Simon, A. Snoch, A. Sochocka, T. Sumikama, H. Suzuki, D. Suzuki, H. Takeda, S. Tangwancharoen, H. Toernqvist, Y. Togano, Z.G. Xiao, S.J. Yennello, Y. Zhang, M.D. Cozma, Probing the symmetry energy with the spectral pion ratio, Phys. Rev. Lett. 126 (2021) 162701, https://doi.org/10.1103/PhysRevLett.126.162701.

[16] M. Cozma, Feasibility of constraining the curvature parameter of the symmetry energy using elliptic flow data, Eur. Phys. J. A 54 (3) (2018) 1–23.

[17] P. Russotto, P. Wu, M. Zoric, M. Chartier, Y. Leifels, R. Lemmon, Q. Li, J. Łukasik, A. Pagano, P. Pawłowski, W. Trautmann, Symmetry energy from elliptic flow in 197Au+197Au, Phys. Lett. B 697 (5) (2011) 471–476, https://doi.org/10.1016/j.physletb.2011.02.033.

[18] P. Russotto, et al., Results of the ASY-EOS experiment at GSI: the symmetry energy at suprasaturation density, Phys. Rev. C 94 (2016) 034608, https://doi.org/10.1103/PhysRevC.94.034608.

[19] J. Margueron, R. Hoffmann Casali, F. Gulminelli, Equation of state for dense nucleonic matter from metamodeling. I. Foundational aspects, Phys. Rev. C 97 (2018) 025805, https://doi.org/10.1103/PhysRevC.97.025805.

[20] Y. Zhang, M. Liu, C.-J. Xia, Z. Li, S.K. Biswal, Constraints on the symmetry energy and its associated parameters from nuclei to neutron stars, Phys. Rev. C 101 (2020) 034303, https://doi.org/10.1103/PhysRevC.101.034303.

[21] B.-A. Li, Constraining the neutron-proton effective mass splitting in neutron-rich matter, Phys. Rev. C 69 (2004) 064602, https://doi.org/10.1103/PhysRevC.69.064602.

[22] K. Brueckner, Cited by 388, Phys. Rev. 97 (5) (1955) 1353–1366, https://doi.org/10.1103/PhysRev.97.1353, https://www.scopus.com/inward/record.uri?eid=2-s2.0-36149019045&doi=10.1103%2fPhysRev.97.1353&partnerID=40&md5=e718dea1d3cc1243be7b9ecff14acd94.

[23] C. Mahaux, P. Bortignon, R. Broglia, C. Dasso, Dynamics of the shell model, Phys. Rep. 120 (1) (1985) 1–274, https://doi.org/10.1016/0370-1573(85)90100-0.

[24] P. Ring, P. Schuck, The Nuclear Many-Body Problem, Springer-Verlag, New York, 1980.

[25] B.-A. Li, B.-J. Cai, L.-W. Chen, J. Xu, Nucleon effective masses in neutron-rich matter, Prog. Part. Nucl. Phys. 99 (2018) 29–119.

[26] J.E. Barney, Charged Pion Emission from ^{112}Sn + ^{124}Sn and ^{124}Sn + ^{112}Sn Reactions with the SπRIT Time Projection Chamber, Ph.D. thesis.

[27] R. Shane, A.B. McIntosh, T. Isobe, W.G. Lynch, H. Baba, J. Barney, Z. Chajecki, M. Chartier, J. Estee, M. Famiano, B. Hong, K. Ieki, G. Jhang, R. Lemmon, F. Lu, T. Murakami, N. Nakatsuka, M. Nishimura, R. Olsen, W. Powell, H. Sakurai, A. Taketani, S. Tangwancharoen, M.B. Tsang, T. Usukura, R. Wang, S.J. Yennello, J. Yurkon, Sπrit: a time-projection chamber for symmetry-energy studies, Nucl. Instrum. Methods Phys. Res., Sect. A, Accel. Spectrom. Detect. Assoc. Equip. 784, Symposium on Radiation Measurements and Applications 2014 (SORMA XV) (2015) 513–517, https://doi.org/10.1016/j.nima.2015.01.026.

[28] J. Estee, W. Lynch, J. Barney, G. Cerizza, G. Jhang, J. Lee, R. Wang, T. Isobe, M. Kaneko, M. Kurata-Nishimura, T. Murakami, R. Shane, S. Tangwancharoen, C. Tsang, M. Tsang, B. Hong, P. Lasko, J. Łukasik, A. McIntosh, P. Pawłowski, K. Pelczar, H. Sakurai, C. Santamaria, D. Suzuki, S. Yennello, Y. Zhang, Extending the dynamic range of electronics in a time projection chamber, Nucl. Instrum. Methods Phys. Res., Sect. A, Accel. Spectrom. Detect. Assoc. Equip. 944 (2019) 162509, https://doi.org/10.1016/j.nima.2019.162509.

[29] J. Lee, G. Jhang, G. Cerizza, J. Barney, J. Estee, T. Isobe, M. Kaneko, M. Kurata-Nishimura, W. Lynch, T. Murakami, C. Tsang, M. Tsang, R. Wang, B. Hong, A. McIntosh, H. Sakurai, C. Santamaria, R. Shane, S. Tangwancharoen, S. Yennello, Y. Zhang, Charged particle track reconstruction with SπRIT time projection chamber, Nucl. Instrum. Methods Phys. Res., Sect. A, Accel. Spectrom. Detect. Assoc. Equip. 965 (2020) 163840, https://doi.org/10.1016/j.nima.2020.163840.

[30] G. Jhang, J. Estee, J. Barney, G. Cerizza, M. Kaneko, J. Lee, W. Lynch, T. Isobe, M. Kurata-Nishimura, T. Murakami, C. Tsang, M. Tsang, R. Wang, D. Ahn, L. Atar, T. Aumann, H. Baba, K. Boretzky, J. Brzychczyk, N. Chiga, N. Fukuda, I. Gasparic, B. Hong, A. Horvat, K. Ieki, N. Inabe, Y. Kim, T. Kobayashi, Y. Kondo, P. Lasko, H. Lee, Y. Leifels, J. Łukasik, J. Manfredi, A. McIntosh, P. Morfouace, T. Nakamura, N. Nakatsuka, S. Nishimura, R. Olsen, H. Otsu, P. Pawłowski, K. Pelczar, D. Rossi, H. Sakurai, C. Santamaria, H. Sato, H. Scheit, R. Shane, Y. Shimizu, H. Simon, A. Snoch, A. Sochocka, Z. Sosin, T. Sumikama, H. Suzuki, D. Suzuki, H. Takeda, S. Tangwancharoen, H. Toernqvist, Y. Togano, Z. Xiao, S. Yennello, J. Yurkon, Y. Zhang, M. Colonna, D. Cozma, P. Danielewicz, H. Elfner, N. Ikeno, C.M. Ko, J. Mohs, D. Oliinychenko, A. Ono, J. Su, Y.J. Wang, H. Wolter, J. Xu, Y.-X. Zhang, Z. Zhang, Symmetry energy investigation with pion production from Sn+Sn systems, Phys. Lett. B 813 (2021) 136016, https://doi.org/10.1016/j.physletb.2020.136016.

[31] M. Kaneko, Hydrogen Isotope Productions in Sn + Sn Collisions with Radioactive Beams at 270 MeV/nucleon, Ph.D. thesis, Kyoto University, 2022.

[32] J.W. Lee, M.B. Tsang, C.Y. Tsang, R. Wang, J. Barney, J. Estee, T. Isobe, M. Kaneko, M. Kurata-Nishimura, W.G. Lynch, T. Murakami, A. Ono, S.R. Souza, D.S. Ahn , L. Atar, T. Aumann, H. Baba, K. Boretzky, J. Brzychczyk, G. Cerizza,

N. Chiga, N. Fukuda, I. Gasparic, B. Hong, A. Horvat, K. Ieki, N. Ikeno, N. Inabe, G. Jhang, Y.J. Kim, T. Kobayashi, Y. Kondo, P. Lasko, H.S. Lee, Y. Leifels, J. Łukasik, J. Manfredi, A.B. McIntosh, P. Morfouace, T. Nakamura, N. Nakatsuka, S. Nishimura, H. Otsu, P. Pawłowski, K. Pelczar, D. Rossi, H. Sakurai, C. Santamaria, H. Sato, H. Scheit, R. Shane, Y. Shimizu, H. Simon, A. Snoch, A. Sochocka, T. Sumikama, H. Suzuki, D. Suzuki, H. Takeda, S. Tangwancharoen, Y. Togano, Z.G. Xiao, S.J. Yennello, Y. Zhang, t.S.p.R. collaboration, Isoscaling in central Sn+Sn collisions at 270 MeV/u, Eur. Phys. J. A 58 (10) (2022) 201, https://doi.org/10.1140/epja/s10050-022-00851-2.

[33] F. Rami, P. Crochet, R. Donà, B. de Schauenburg, P. Wagner, J. Alard, A. Andronic, Z. Basrak, N. Bastid, I. Belyaev, A. Bendarag, G. Berek, D. Best, R. Čaplar, A. Devismes, P. Dupieux, M. Dželalija, M. Eskef, Z. Fodor, A. Gobbi, Y. Grishkin, N. Herrmann, K. Hildenbrand, B. Hong, J. Kecskemeti, M. Kirejczyk, M. Korolija, R. Kotte, A. Lebedev, Y. Leifels, H. Merlitz, S. Mohren, D. Moisa, W. Neubert, D. Pelte, M. Petrovici, C. Pinkenburg, C. Plettner, W. Reisdorf, D. Schüll, Z. Seres, B. Sikora, V. Simion, K. Siwek-Wilczyńska, G. Stoicea, M. Stockmeir, M. Vasiliev, K. Wisniewski, D. Wohlfarth, I. Yushmanov, A. Zhilin, Flow angle from intermediate mass fragment measurements, Nucl. Phys. A 646 (3) (1999) 367–384, https://doi.org/10.1016/S0375-9474(98)00641-1.

[34] A. Andronic, W. Reisdorf, J.P. Alard, V. Barret, Z. Basrak, N. Bastid, A. Bendarag, G. Berek, R. Čaplar, P. Crochet, A. Devismes, P. Dupieux, M. Dželalija, C. Finck, Z. Fodor, A. Gobbi, Y. Grishkin, O.N. Hartmann, N. Herrmann, K.D. Hildenbrand, B. Hong, J. Kecskemeti, Y.J. Kim, M. Kirejczyk, P. Koczon, M. Korolija, R. Kotte, T. Kress, R. Kutsche, A. Lebedev, Y. Leifels, W. Neubert, D. Pelte, M. Petrovici, F. Rami, B. de Schauenburg, D. Schüll, Z. Seres, B. Sikora, K.S. Sim, V. Simion, K. Siwek-Wilczyńska, V. Smolyankin, M.R. Stockmeier, G. Stoicea, P. Wagner, K. Wiśniewski, D. Wohlfarth, I. Yushmanov, A. Zhilin, Differential directed flow in Au+Au collisions, Phys. Rev. C 64 (2001) 041604, https://doi.org/10.1103/PhysRevC.64.041604.

[35] E. De Filippo, P. Russotto, L. Acosta, M. Adamczyk, A. Al-Ajlan, M. Al-Garawi, S. Al-Homaidhi, F. Amorini, L. Auditore, T. Aumann, Y. Ayyad, Z. Basrak, J. Benlliure, M. Boisjoli, K. Boretzky, J. Brzychczyk, A. Budzanowski, C. Caesar, G. Cardella, P. Cammarata, Z. Chajecki, M. Chartier, A. Chbihi, M. Colonna, M.D. Cozma, B. Czech, M. Di Toro, M. Famiano, S. Gannon, I. Gaspari´c, L. Grassi, C. Guazzoni, P. Guazzoni, M. Heil, L. Heilborn, R. Introzzi, T. Isobe, K. Kezzar, M. Kis, A. Krasznahorkay, S. Kupny, N. Kurz, E. La Guidara, G. Lanzalone, P. Lasko, A. Le Fèvre, Y. Leifels, R.C. Lemmon, Q.F. Li, I. Lombardo, J. Lukasik, W.G. Lynch, P. Marini, Z. Matthews, L. May, T. Minniti, M. Mostazo, A. Pagano, E.V. Pagano, M. Papa, P. Pawlowski, S. Pirrone, G. Politi, F. Porto, W. Reviol, F. Riccio, F. Rizzo, E. Rosato, D. Rossi, S. Santoro, D.G. Sarantites, H. Simon, I. Skwirczynska, Z. Sosin, L. Stuhl, W. Trautmann, A. Trifirò, M. Trimarchi, M.B. Tsang, G. Verde, M. Veselsky, M. Vigilante, Yongjia Wang, A. Wieloch, The symmetry energy at suprasaturation density and the ASY-EOS experiment at GSI, EPJ Web Conf. 137 (2017) 09002, https://doi.org/10.1051/epjconf/201713709002.

[36] A. Le Fevre, Y. Leifels, W. Reisdorf, J. Aichelin, C. Hartnack, Constraining the nuclear matter equation of state around twice saturation density, Nucl. Phys. A 945 (2016) 112–133.

[37] P. Russotto, M.D. Cozma, E.D. Filippo, A.L. Fèvre, Y. Leifels, J. Łukasik, Studies of the equation-of-state of nuclear matter by heavy-ion collisions at intermediate energy in the multi-messenger era, Riv. Nuovo Cimento 46 (1) (2023) 1–70, https://doi.org/10.1007/s40766-023-00039-4.

[38] G. Stoicea, M. Petrovici, A. Andronic, N. Herrmann, J.P. Alard, Z. Basrak, V. Barret, N. Bastid, R. Čaplar, P. Crochet, P. Dupieux, M. Dželalija, Z. Fodor, O. Hartmann, K.D. Hildenbrand, B. Hong, J. Kecskemeti, Y.J. Kim, M. Kirejczyk, M. Korolija, R. Kotte, T. Kress, A. Lebedev, Y. Leifels, X. Lopez, M. Merschmeier, W. Neubert, D. Pelte, F. Rami, W. Reisdorf, D. Schüll, Z. Seres, B. Sikora, K.S. Sim, V. Simion, K. Siwek-Wilczyńska, V. Smolyankin, M. Stockmeier, K. Wiśniewski, D. Wohlfarth, I. Yushmanov, A. Zhilin, P. Danielewicz, Azimuthal dependence of collective expansion for symmetric heavy-ion collisions, Phys. Rev. Lett. 92 (2004) 072303, https://doi.org/10.1103/PhysRevLett.92.072303.

[39] W. Reisdorf, Y. Leifels, A. Andronic, R. Averbeck, V. Barret, Z. Basrak, N. Bastid, M. Benabderrahmane, R. Čaplar, P. Crochet, P. Dupieux, M. Dželalija, Z. Fodor, P. Gasik, Y. Grishkin, O. Hartmann, N. Herrmann, K. Hildenbrand, B. Hong, T. Kang, J. Kecskemeti, Y. Kim, M. Kirejczyk, M. Kiš, P. Koczoń, M. Korolija, R. Kotte, T. Kress, A. Lebedev, X. Lopez, T. Matulewicz, M. Merschmeyer, W. Neubert, M. Petrovici, K. Piasecki, F. Rami, M. Ryu, A. Schüttauf, Z. Seres, B. Sikora, K. Sim, V. Simion, K. Siwek-Wilczyńska, V. Smolyankin, M. Stockmeier, G. Stoicea, Z. Tymiński, K. Wiśniewski, D. Wohlfarth, Z. Xiao, H. Xu, I. Yushmanov, A. Zhilin, Systematics of azimuthal asymmetries in heavy ion collisions in the 1a gev regime, Nucl. Phys. A 876 (2012) 1–60, https://doi.org/10.1016/j.nuclphysa.2011.12.006.

[40] S. Voloshin, Y. Zhang, Flow study in relativistic nuclear collisions by Fourier expansion of azimuthal particle distributions, Z. Phys. C, Part. Fields 70 (4) (1996) 665–671, https://doi.org/10.1007/s002880050141.

[41] A.M. Poskanzer, S.A. Voloshin, Methods for analyzing anisotropic flow in relativistic nuclear collisions, Phys. Rev. C 58 (1998) 1671–1678, https://doi.org/10.1103/PhysRevC.58.1671.

[42] A. Ono, Dynamics of clusters and fragments in heavy-ion collisions, Prog. Part. Nucl. Phys. 105 (2019) 139–179, https://doi.org/10.1016/j.ppnp.2018.11.001.

[43] B. Dönigus, Selected highlights of the production of light (anti-) (hyper-)nuclei in ultra-relativistic heavy-ion collisions, Eur. Phys. J. A 56 (11) (2020) 280, https://doi.org/10.1140/epja/s10050-020-00275-w.

[44] P. Gossiaux, R. Puri, C. Hartnack, J. Aichelin, The multifragmentation of spectator matter, Nucl. Phys. A 619 (3) (1997) 379–390, https://doi.org/10.1016/S0375-9474(97)00175-9.

[45] X. Chen, Y. Zhang, Z. li, Theoretical uncertainties on the extraction of in-medium NN cross sections by different Pauli blocking algorithms, Chin. Phys. C (Apr 2021), https://doi.org/10.1088/1674-1137/abfb51.

[46] P. Li, Y. Wang, Q. Li, H. Zhang, Accessing the in-medium effects on nucleon-nucleon elastic cross section with collective flows and nuclear stopping, Phys. Lett. B 828 (2022) 137019, https://doi.org/10.1016/j.physletb.2022.137019.

[47] W. Reisdorf, A. Andronic, R. Averbeck, M. Benabderrahmane, O. Hartmann, N. Herrmann, K. Hildenbrand, T. Kang, Y. Kim, M. Kiš, P. Koczoń, T. Kress, Y. Leifels, M. Merschmeyer, K. Piasecki, A. Schüttauf, M. Stockmeier, V. Barret, Z. Basrak, N. Bastid, R. Čaplar, P. Crochet, P. Dupieux, M. Dželalija, Z. Fodor, P. Gasik, Y. Grishkin, B. Hong, J. Kecskemeti, M. Kirejczyk, M. Korolija, R. Kotte, A. Lebedev, X. Lopez, T. Matulewicz, W. Neubert, M. Petrovici, F. Rami, M. Ryu, Z. Seres, B. Sikora, K. Sim, V. Simion, K. Siwek-Wilczyńska, V. Smolyankin, G. Stoicea, Z. Tymiński, K. Wiśniewski, D. Wohlfarth, Z. Xiao, H. Xu, I. Yushmanov, A. Zhilin, Systematics of central heavy ion collisions in the 1A GeV regime, Nucl. Phys. A 848 (3) (2010) 366–427, https://doi.org/10.1016/j.nuclphysa.2010.09.008.

[48] T. Gaitanos, C. Fuchs, H. Wolter, Nuclear stopping and flow in heavy-ion collisions and the in-medium NN cross section, Phys. Lett. B 609 (3) (2005) 241–246, https://doi.org/10.1016/j.physletb.2005.01.069.

[49] J. Barney, J. Estee, W.G. Lynch, T. Isobe, G. Jhang, M. Kurata-Nishimura, A.B. McIntosh, T. Murakami, R. Shane, S. Tangwancharoen, M.B. Tsang, G. Cerizza, M. Kaneko, J.W. Lee, C.Y. Tsang, R. Wang, C. Anderson, H. Baba, Z. Chajecki, M. Famiano, R. Hodges-Showalter, B. Hong, T. Kobayashi, P. Lasko, J. Łukasik, N. Nakatsuka, R. Olsen, H. Otsu, P. Pawłowski, K. Pelczar, H. Sakurai, C. Santamaria, H. Setiawan, A. Taketani, J.R. Winkelbauer, Z. Xiao, S.J. Yennello, J. Yurkon, Y. Zhang, The SπRIT time projection chamber, Rev. Sci. Instrum. 92 (6) (2021), https://doi.org/10.1063/5.0041191, https://www.osti.gov/biblio/1797552.

[50] M. Kaneko, T. Murakami, T. Isobe, M. Kurata-Nishimura, A. Ono, N. Ikeno, J. Barney, G. Cerizza, J. Estee, G. Jhang, J. Lee, W. Lynch, C. Santamaria, C. Tsang, M. Tsang, R. Wang, D. Ahn, L. Atar, T. Aumann, H. Baba, K. Boretzky, J. Brzychczyk, N. Chiga, N. Fukuda, I. Gašparić, B. Hong, A. Horvat, T. Ichihara, K. Ieki, N. Inabe, Y. Kim, T. Kobayashi, Y. Kondo, P. Lasko, H. Lee, Y. Leifels, J. Łukasik, J. Manfredi, A. McIntosh, P. Morfouace, T. Nakamura, N. Nakatsuka, S. Nishimura, R. Olsen, H. Otsu, P. Pawłowski, K. Pelczar, D. Rossi, H. Sakurai, H. Sato, H. Scheit, R. Shane, Y. Shimizu, H. Simon, T. Sumikama, D. Suzuki, H. Suzuki, H. Takeda, S. Tangwancharoen, Y. Togano, H. Törnqvist, Z. Xiao, S. Yennello, J. Yurkon, Y. Zhang, Rapidity distributions of Z = 1 isotopes and the nuclear symmetry energy from Sn+Sn collisions with radioactive beams at 270 MeV/nucleon, Phys. Lett. B 822 (2021) 136681, https://doi.org/10.1016/j.physletb.2021.136681.

[51] Y. Zhang, M. Tsang, Z. Li, H. Liu, Constraints on nucleon effective mass splitting with heavy ion collisions, Phys. Lett. B 732 (2014) 186–190, https://doi.org/10.1016/j.physletb.2014.03.030.

[52] Y. Zhang, M. Tsang, Z. Li, Covariance analysis of symmetry energy observables from heavy ion collision, Phys. Lett. B 749 (2015) 262–266, https://doi.org/10.1016/j.physletb.2015.07.064.

[53] T.H.R. Skyrme, CVII. The nuclear surface, Philos. Mag.: J. Theor. Exp. Appl. Phys. 1 (11) (1956) 1043–1054, https://doi.org/10.1080/14786435608238186.

[54] D. Vautherin, D.M. Brink, Hartree-Fock calculations with Skyrme's interaction. I. Spherical nuclei, Phys. Rev. C 5 (1972) 626–647, https://doi.org/10.1103/PhysRevC.5.626.

[55] E. Chabanat, P. Bonche, P. Haensel, J. Meyer, R. Schaeffer, A Skyrme parametrization from subnuclear to neutron star densities, Nucl. Phys. A 627 (4) (1997) 710–746, https://doi.org/10.1016/S0375-9474(97)00596-4.

[56] B.K. Agrawal, S. Shlomo, V.K. Au, Determination of the parameters of a Skyrme type effective interaction using the simulated annealing approach, Phys. Rev. C 72 (2005) 014310, https://doi.org/10.1103/PhysRevC.72.014310.

[57] L.-W. Chen, B.-J. Cai, C.M. Ko, B.-A. Li, C. Shen, J. Xu, Higher-order effects on the incompressibility of isospin asymmetric nuclear matter, Phys. Rev. C 80 (2009) 014322, https://doi.org/10.1103/PhysRevC.80.014322.

[58] J. Cugnon, D. L'Hôte, J. Vandermeulen, Nucl. Instrum. Methods Phys. Res., Sect. B, Beam Interact. Mater. Atoms 111 (3–4) (1996) 215–220, https://doi.org/10.1016/0168-583X(95)01384-9, cited by 95, https://www.scopus.com/inward/record.uri?eid=2-s2.0-0030143153&doi=10.1016%2f0168-583X%2895%2901384-9&partnerID=40&md5=e6854ad674cc549da0dbc3c211cefbf0.

[59] A. Patil, D. Huard, C.J. Fonnesbeck, PyMC: Bayesian stochastic modelling in python, J. Stat. Softw. 35 (4) (2010) 1–81, 21603108[pmid], https://pubmed.ncbi.nlm.nih.gov/21603108.

[60] C.E. Rasmussen, C.K.I. Williams, in: Gaussian Processes for Machine Learning (Adaptive Computation and Machine Learning), 2005.

[61] B.-A. Li, B.-J. Cai, L.-W. Chen, W.-J. Xie, J. Xu, N.-B. Zhang, A theoretical overview of isospin and eos effects in heavy-ion reactions at intermediate energies, Il Nuovo Cimento C 45 (3) (2022), https://doi.org/10.1393/ncc/i2022-22054-3.

[62] H. Wolter, M. Colonna, D. Cozma, P. Danielewicz, C.M. Ko, R. Kumar, A. Ono, M.B. Tsang, J. Xu, Y.-X. Zhang, E. Bratkovskaya, Z.-Q. Feng, T. Gaitanos, A.L. Fèvre, N. Ikeno, Y. Kim, S. Mallik, P. Napolitani, D. Oliinychenko, T. Ogawa, M. Papa, J. Su, R. Wang, Y.-J. Wang, J. Weil, F.-S. Zhang, G.-Q. Zhang, Z. Zhang, J. Aichelin, W. Cassing, L.-W. Chen, H.-G. Cheng, H. Elfner, K. Gallmeister, C. Hartnack, S. Hashimoto, S. Jeon, K. Kim, M. Kim, B.-A. Li, C.-H. Lee, Q.-F. Li, Z.-X. Li, U. Mosel, Y. Nara, K. Niita, A. Ohnishi, T. Sato, T. Song, A. Sorensen, N. Wang, W.-J. Xie, Transport model comparison studies of intermediate-energy heavy-ion collisions, arXiv:2202.06672, 2022.